Polyhedron 228 (2022) 116178

Contents lists available at ScienceDirect

Polyhedron

journal homepage: www.elsevier.com/locate/poly

Polypyridyl coordinated rhenium(I) tricarbonyl complexes as model devices for cancer diagnosis and treatment

Lehlohonolo Moherane [a], Orbett T. Alexander [b], Marietjie Schutte-Smith [b], Robin E. Kroon [c], Penny P. Mokolokolo [b], Supratim Biswas [d], Sharon Prince [d], Hendrik G. Visser [b], Amanda-Lee E. Manicum [a,*]

[a] Department of Chemistry, Tshwane University of Technology, PO Box X680, Pretoria 0001, South Africa
[b] Department of Chemistry, University of the Free State, PO Box 339, Bloemfontein 9300, South Africa
[c] Department of Physics, University of the Free State, PO Box 339, Bloemfontein 9300, South Africa
[d] Department of Human Biology, University of Cape Town, Anzio Road Observatory, 7925 Cape Town, South Africa

ARTICLE INFO

Keywords:
Rhenium(I) tricarbonyl
N,N′-bidentate
Phosphines
Photoluminescence
Cytotoxicity

ABSTRACT

This study reports on the solid-state structures, solution-state photoluminescence and *in vitro* biological applications of *fac*-[Re(CO)$_3$(*N,N′*-Bid)(X)]^n where *N,N′*-Bid = 4,4′-dimethyl-2,2′-bipyridine, 5,5′-dimethyl-2,2′-bipyridine and 4,4′-dimethoxy-2,2′-bipyridine; X = triphenylphosphine, dicyclohexylphenylphosphine, cyclohexyldiphenylphosphine, 1,3,5 triaza-7-phosphaadamantane, OH$_2$ and Br, and n = 0, +1. All the synthesised complexes (**1**–**18**) were spectroscopically characterized using infrared, nuclear magnetic resonance (^{1}H, ^{13}C and ^{31}P) and ultraviolet/visible techniques, and single crystal X-ray diffraction. An increasing trend was noted in the IR CO stretching frequencies, *fac*-[Re(CO)$_3$(*N,N′*-Bid)(Br)] > *fac*-[Re(CO)$_3$(*N,N′*-Bid)(H$_2$O)]$^+$ > *fac*-[Re(CO)$_3$(*N,N′*-Bid)(P)]$^+$. The study reports three new crystal structures: *fac*-[Re(CO)$_3$(5,5′-DiMBpy)(NO$_3$)] (**2a**), *fac*-[Re(CO)$_3$(4,4′-DiMoxBpy)(NO$_3$)][(CH$_3$)$_2$CO] (**3a**) and *fac*-[Re(CO)$_3$(4,4′-DiMBpy)(Br)] (**4**). The ligand bite angles (*N*-Re-N) are 74.8(2)° for **2a**, 74.57(13)° for **3a** and 74.80(2)° for **4**. All eighteen complexes displayed excellent luminescent properties, with an emission range between 505 and 609 nm, and the most significant Stokes shift of 270 nm is noted for **3**. *In vitro* biological screening against breast cancers revealed two viable complexes, *fac*-[Re(CO)$_3$(4,4′-DiMoxBpy)(Br)] (**6**) with IC$_{50}$ = 10.92 ± 2.3 μM against MDA-MB-231 cells (SI = 1.49) and IC$_{50}$ = 16.25 ± 1.9 μM against MRC-5 cells; *fac*-[Re(CO)$_3$(5,5′-DiMBpy)(CyPh$_2$P]$^+$ (**13**) with IC$_{50}$ = 5.74 ± 2.5 μM against MCF-7 cells (SI = 2.62) and IC$_{50}$ = 15.04 ± 2.6 μM against MRC-5 cells.

1. Introduction

Photodynamic therapy (PDT) and molecular imaging (MI) have displayed potential as effective complementary or alternative cancer diagnostic and treatment methods [1–3], following Raab's work on the effects of visible light and acridine dye [4]. The PDT process begins with administering a photosensitizer (PS); this is usually a photoactivatable molecule that can be activated by irradiation with light at a specific wavelength. There are, however, weaknesses that exist with the current PS molecules for PDT due to insolubility issues and conglomeration within physiological environments [5,6], which indicates the need for new PDT agents. Molecular imaging, on the other hand, involves the imaging of molecules with medical significance within living organisms and it is a critical area in which late-transition metal complexes can be applied. For example, polypyridyl complexes involving metals such as Re [7–9] and Ru [10,11] have shown practical applications in molecular imaging, with Ir [12,13] showing practical applications in cellular imaging studies. This is, therefore, the justification behind this study, in which polypyridyl ligands are coordinated to the Re(I) tricarbonyl metal core, because previous studies indicated the rich photophysical and biochemical properties of these complexes as possible agents for PDT [14,15]. Furthermore, as potential MI probes, Re(I) complexes have displayed optimal polarized emission, increased photostability, large Stokes shifts, excellent biocompatibility and cytotoxic potential towards cancer cells [16–19].

Therefore, this work was aimed at investigating the solution state luminescence and biological applications of polypyridyl coordinated Re(I) complexes for cancer therapy. Different functionalized 2,2′-

* Corresponding author.
E-mail address: ManicumAE@tut.ac.za (A.-L.E. Manicum).

https://doi.org/10.1016/j.poly.2022.116178
Received 26 July 2022; Accepted 11 October 2022
Available online 21 October 2022

bipyridine *N,N′*-donor bidentate ligands were used, namely 5,5′-dimethyl-2,2′-bipyridine (5,5′-DiMBpy), 4,4′-dimethyl-2,2′-bipyridine (4,4′-DiMBpy) and 4,4′-dimethoxy-2,2′-bipyridine (4,4′-DiMoxBpy). The monodentate ligands used were four *P*-donor ligands, triphenylphosphine (PPh_3), dicyclohexylphenylphosphine (Cy_2PhP), cyclohexyldiphenylphosphine ($CyPh_2P$) and 1,3,5 triaza-7-phosphaadamantane (PTA). The crystallographic study and photoluminescence investigations provided insight into the synthesized complexes' solid-state molecular structures and MI potential. The *in vitro* biological study shed light on applying three synthesized complexes to female-related cancers, i.e. triple negative MDA-MB-231 and MCF-7 breast cancers.

2. Experimental

2.1. Materials and methods

All the chemicals used for the synthesis and characterization were reagent grade and used without further purification. Chemicals were purchased from Sigma-Aldrich, South Africa unless stated otherwise. All solvents used were purified and dried by following the procedure prescribed by Perrin *et al.* (1966) for dry conditions [20]. Schlenk line methods were used for all reactions that were either moisture or air sensitive. Rhenium pentacarbonyl bromide was bought from Strem Chemicals, Newburyport (USA). The precursor, *fac*-$[NEt_4]_2[Re(CO)_3(Br)_3]$, used for the aqua complexes, was synthesized according to the procedure provided by Roger Alberto *et al.* (1994) [21]. All the ligands were bought from Sigma-Aldrich and will be abbreviated. Nitric acid (HNO_3) was used to adjust the pH during the synthesis of the aqua complexes. The UV/Vis analysis was performed on a Varian Cary 50 Conc UV/Visible spectrophotometer equipped with a Julabo F12mV temperature cell regulator (accurate to within 0.1 °C) in a 1.000 ± 0.001 cm quartz cuvette cell. The infrared spectra of the complexes were recorded on a Bruker Tensor 27 Standard System spectrophotometer with a laser range of 4000–370 cm^{-1}, which was coupled to a computer. The IR spectrometer was equipped with a temperature cell regulator, accurate to within 0.3 °C. KBr pellets were used for solid samples. All Nuclear Magnetic Resonance (NMR) spectra were recorded on a Bruker 300 MHz NMR spectrometer operating at 300 MHz, using deuterated solvents or samples spiked with deuterated solvent. All the chemical shifts, δ, are reported in ppm (part per million) using TMS (tetramethylsilane) as the internal standard for ^1H NMR and phosphoric acid as an external reference for ^{31}P NMR. Coupling constants, *J*, are reported in Hertz (Hz). For the *in vitro* biological study, the complexes were soluble in DMSO after heating and no precipitates were observed in the cell medium after adding them to the cells. Furthermore, for the stability determination of complexes **1**–**18** in DMSO, their solution UV/Vis spectra were regularly recorded over several days.

2.2. Synthesis of the complexes

The synthesis of the starting synthon, *fac*-$[NEt_4]_2[Re(CO)_3(Br)_3]$, was strictly performed under Schlenk conditions. The reported complexes were synthesized according to published procedures [22,23], and Scheme 1 summarizes the synthetic routes.

fac-$[NEt_4]_2[Re(CO)_3(Br)_3]$ (251 mg, 0.325 mmol) was stirred in 15 ml of water at pH 2.2 for 30 min until it dissolved. Next, $AgNO_3$ (163 mg, 0.962 mmol) was added to the solution and stirred for 24 h at room temperature. The formed precipitate, AgBr (183 mg, 0.975 mmol), was filtered off and weighed. This was followed by adding the respective polypyridyl ligands 4,4′-dimethyl-2,2-bipyridyl (120 mg, 0.649 mmol), 5,5′-dimethyl-2,2-bipyridyl (119 mg, 0.648 mmol) and 4,4′-dimethoxy-2,2-bipyridyl (112 mg, 0.519 mmol) to the filtrate and stirring for 36 h at room temperature. The light-yellow precipitates (product) that formed were filtered off, dried, recrystallized and weighed to yield complexes **1**–**3**, **2a** and **3a**.

The bromide coordinated complexes (**4**–**6**) were synthesised as follows: *fac*-$[NEt_4]_2[Re(CO)_3(Br)_3]$ (~200 mg, 0.260 mmol) was dissolved in water (20 ml) and respectively added to 4,4′-dimethyl-2,2′-bipyridine (96 mg, 0.518 mmol), 5,5′-dimethyl-2,2′-bipyridine (95 mg, 0.518 mmol) and 4,4′-dimethoxy-2.2-bipyridyl dissolved in ethanol (6 ml). The solution was stirred for 48 h, then the solvent was filtered off. The yellow solid obtained was washed with water, cold ethanol and petroleum ether, then allowed to air-dry. **7**, **11** and **15** were synthesized by respectively dissolving **1** (25 mg; 0.0528 mmol), **2** (26 mg; 0.0555 mmol) and **3** (31 mg; 0.0603 mmol) in methanol (10 ml) and adding PPh_3 (14 mg; 0.0545 mmol) dissolved in methanol (5 ml). The solution was stirred at 80 °C for 48 h and the dark brown solution obtained was concentrated by evaporation of the solvent. The precipitate obtained from solvent evaporation was washed with methanol to dissolve the excess PPh_3. The product was dried and weighed. **8**, **12** and **16** were separately synthesized by dissolving **1** (25 mg; 0.053 mmol), **2** (25 mg;

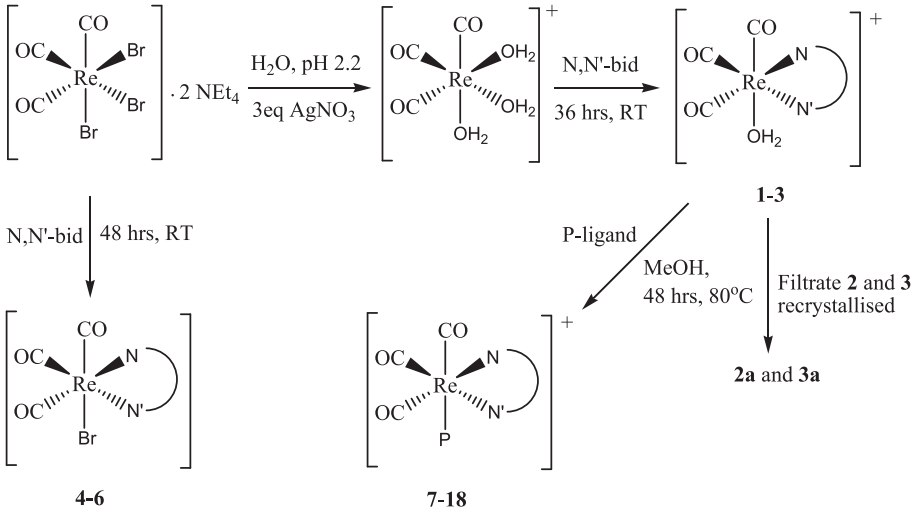

Scheme 1. A schematic presentation of the synthetic approach for complexes **1**–**18**.

0.053 mmol) and **3** (50 mg; 0.099 mmol) in methanol (10 ml) and adding one equivalent of PTA dissolved in methanol. The solution was stirred at 80 °C for 48 h and the yellow solution that was obtained was concentrated by evaporation of the solvent. The precipitate obtained from solvent evaporation was washed with methanol to dissolve the excess PTA and the product was dried and weighed. **9**, **13** and **17** were synthesized by dissolving **1** (25 mg; 0.053 mmol), **2** (25 mg; 0.053 mmol) and **3** (30 mg; 0.059 mmol) in methanol and adding $CyPh_2P$ (14 mg; 0.054 mmol) dissolved in methanol (5 ml). The solution was stirred at 80 °C for 48 h and the dark orange solution was concentrated by evaporation of the solvent. The precipitate obtained from solvent evaporation was washed with methanol to dissolve the excess $CyPh_2P$. **10**, **14** and **18** were synthesized by dissolving **1** (25 mg; 0.053 mmol), **2** (50 mg; 0.087 mmol) and **3** (31 mg; 0.060 mmol) in methanol (10 ml) and one equivalent of Cy_2PhP (15 mg; 0.0530 mmol) dissolved in methanol was added. The solution was stirred at 80 °C for 48 h and the dark orange solution was concentrated by evaporation of the solvent. The precipitate obtained from solvent evaporation was washed with methanol to dissolve the excess Cy_2PhP. The product was dried and weighed.

*fac-[Re(CO)$_3$(4,4′-DiMBpy)(H$_2$O)][NO$_3$] (**1**)*. Yield: 120 mg, 77.88 %; ^{1}H NMR (400 MHz, $CDCl_3$), δ (ppm): 8.93–8.91 (d, $J = 6$ Hz, H6/6′), 8.00 (s, 2H, H3/3′), 7.35–7.34 (d, $J = 6$ Hz, 2H, H5/5′), 2.61 (s, 6H, 4,4′-2xCH_3); ^{13}C NMR (151 MHz, CD_2Cl_2), δ (ppm): 155.5, 153.2, 153.7, 128.1, 123.9, 21.5; IR (KBr, cm^{-1}), ν_{CO}: 2023, 1914, 1868; UV/Vis, λ^{max}, nm (ε, M^{-1} cm^{-1}): 360 (3680); Anal. Calc. for $C_{15}H_{17}N_3O_7Re$: C, 33.52; H, 3.19; N, 7.82; Found: C, 33.50; H, 3.21; N, 7.77 %.

*fac-[Re(CO)$_3$(5,5′-DiMBpy)(H$_2$O)][NO$_3$] (**2**) and (**2a**)*. From the filtrate of **2**, crystals suitable for single-crystal X-ray diffraction characterization were obtained and collected. The molecular structure of *fac*-[Re(CO)$_3$(5,5′-DiMBpy)(NO$_3$)] (**2a**) was confirmed with XRD and the data is reported in the crystallography section. Yield: 128 mg, 82.82 %; ^{1}H NMR (400 MHz, $CDCl_3$), δ (ppm): 8.92 (s, 2H, H6/6′), 8.11–8.09 (d, $J = 8$ Hz, 2H, H3/3′), 7.97–7.95 (dd, $J = 2$ Hz, $J = 8$ Hz, 2H, H4/4′), 2.55 (s, 6H, 5,5′-2xCH_3); ^{13}C NMR (151 MHz, CD_2Cl_2), δ (ppm): 186.7, 153.8, 140.4, 138.3, 122.3, 18.3; IR (KBr, cm^{-1}), ν_{CO}: 2017, 1888; UV/Vis, λ^{max}, nm (ε, M^{-1} cm^{-1}): 355 (3235); Anal. Calc. for $C_{15}H_{17}N_3O_7Re$: C, 33.52; H, 3.19; N, 7.82; Found: C, 33.48; H, 3.16; N, 7.79 %.

*fac-[Re(CO)$_3$(4,4′-DiMoxBpy)(H$_2$O)][NO$_3$] (**3**) and (**3a**)*. From the filtrate of **3**, crystals suitable for single-crystal X-ray diffraction characterization were obtained and collected. The molecular structure of *fac*-[Re(CO)$_3$(4,4′-DiMoxBpy)(NO$_3$)][$(CH_3)_2CO$] (**3a**) was confirmed with XRD and the data is reported in the crystallography section. Yield: 189 mg, 71.80 %; ^{1}H NMR (400 MHz, $CDCl_3$), δ (ppm): 8.99–8.88 (d, $J = 6$ Hz, 2H, H6/6′), 7.56–7.55 (d, $J = 3$ Hz, 2H, H3/3′), 7.02–6.99 (dd, $J = 3$ Hz, $J = 6$ Hz, 2H, H5/5′), 4.04 (s, 6H, 4,4′-2xOCH_3); ^{13}C NMR (151 MHz, $CDCl_3$), δ (ppm): 162.4, 156.4, 125.4, 124.8, 105.7, 104.4, 59.4; IR (KBr, cm^{-1}), ν_{CO}: 2024, 1886; UV/Vis, λ^{max}, nm (ε, M^{-1} cm^{-1}): 350 (3995); Anal. Calc. for $C_{15}H_{17}N_3O_9Re$: C, 31.63; H, 3.01; N, 7.38; Found: C, 31.60; H, 2.99; N, 7.36 %.

*fac-[Re(CO)$_3$(4,4′-DiMBpy)(Br)] (**4**)*. The precipitate was recrystallized from hexane and dichloromethane in a 1:1 ratio to yield **4** and this was confirmed with single-crystal X-ray diffraction. Yield: 112 mg, 79.91 %; ^{1}H NMR (300 MHz, $CDCl_3$), δ (ppm): 8.92–8.90 (d, $J = 6$ Hz, 2H, H6/6′), 7.99 (s, 2H, H3/3′), 7.35–7.33 (d, $J = 4$ Hz, 2H, H5/5′), 2.60 (s, 6H, 4,4′-2xCH_3); ^{13}C NMR (151 MHz, CD_2Cl_2), δ (ppm): 155.3, 152.5, 151.7, 148.8, 127.9, 123.9, 21.4; IR (KBr, cm^{-1}), ν_{CO}: 2013, 1881, 1864; UV/Vis, λ^{max}, nm (ε, M^{-1} cm^{-1}): 380 (3685); Anal. Calc. for $C_{15}H_{15}BrN_2O_3Re$: C, 33.52; H, 2.81; N, 5.21; Found: C, 33.51; H, 2.83; N, 5.19 %.

*fac-[Re(CO)$_3$(5,5′-DiMBpy)(Br)] (**5**)*. Yield: 101 mg, 72.01 %; ^{1}H NMR (300 MHz, $CDCl_3$), δ (ppm): 8.88 (s, 2H, H6/6′), 8.05–8.02 (d, $J = 8$ Hz, 2H, H3/3′), 7.86–7.82 (dd, $J = 2$ Hz, $J = 8$ Hz, 2H, H4/4′), 2.52 (s, 6H, 5,5′-2xCH_3); ^{13}C NMR (151 MHz, CD_2Cl_2), δ (ppm): 153.1, 139.6, 137.8, 122.3, 18.3; IR (KBr, cm^{-1}), ν_{CO}: 2018, 1934, 1897; UV/Vis, λ^{max}, nm (ε, M^{-1} cm^{-1}): 375 (2925); Anal. Calc. for $C_{15}H_{15}BrN_2O_3Re$: C, 33.52; H, 2.81; N, 5.21; Found: C, 33.49; H, 2.79; N, 5.23 %.

*fac-[Re(CO)$_3$(4,4′-DiMoxBpy)(Br)] (**6**)*. Yield: 70 mg, 62.85 %; ^{1}H NMR (400 MHz, $CDCl_3$), δ (ppm): 8.87–8.84 (dd, $J = 5$ Hz, $J = 6$ Hz, 2H, H6/6′), 7.57–7.56 (d, $J = 2$ Hz, 2H, H3/3′), 7.02–6.99 (m, 2H, H5/5′), 4.04 (s, 6H, 4,4′-2xOCH_3); ^{13}C NMR (151 MHz, $CDCl_3$), δ (ppm): 167.5, 157.2, 154.6, 154.4, 112.1, 110.3, 56.5; IR (KBr, cm^{-1}), ν_{CO} : 2021, 1876; UV/Vis, λ^{max}, nm (ε, M^{-1} cm^{-1}): 365 (4720); Anal. Calc. for $C_{15}H_{15}BrN_2O_5Re$: C, 31.64; H, 2.66; N, 4.92; Found: C, 31.60; H, 2.64; N, 4.90 %.

*fac-[Re(CO)$_3$(4,4′-DiMBpy)(PPh$_3$)][NO$_3$] (**7**)*. Yield: 30 mg, 81.35 %; ^{1}H NMR (400 MHz, $CDCl_3$), δ (ppm): 8.96–8.94 (d, $J = 8$ Hz, 2H, H6/6′), 7.99 (s, 2H, H3/3′), 7.72–7.66 (m, 6H, -PPh_3), 7.59–7.55 (t, $J = 7$ Hz, 3H, -PPh_3), 7.51–7.46 (ddd, $J = 3$ Hz, $J = 3$ Hz, $J = 2.8$ Hz, 6H, -PPh_3), 7.39–7.37 (d, $J = 5$ Hz, 2H, H5/5′), 2.60 (s, 6H, 4,4′-2xCH_3); ^{13}C NMR (151 MHz, $CDCl_3$), δ (ppm): 155.7, 153.5, 152.6, 152.2, 132.7, 132.2, 132.1, 132.0, 128.6, 128.5, 128.2, 123.9, 22.0, 21.8; ^{31}P NMR (400 MHz, $CDCl_3$), δ (ppm): 29.1; IR (KBr, cm^{-1}), ν_{CO} : 2025, 1909, UV/Vis, λ^{max}, nm (ε, M^{-1} cm^{-1}): 347 (3860); Anal. Calc. for $C_{33}H_{30}N_3O_6Re$: C, 50.70; H, 3.87; N, 5.37; Found: C, 50.69; H, 3.85; N, 5.35 %.

*fac-[Re(CO)$_3$(4,4′-DiMBpy)(PTA)][NO$_3$] (**8**)*. Yield: 25 mg, 78.01 %; ^{1}H NMR (400 MHz, $CDCl_3$), δ (ppm): 8.78–8.76 (d, $J = 8$ Hz, 2H, H6/6′), 8.68 (s, 2H, H3/3′), 8.12 (d, $J = 8$ Hz, 2H, H5/5′), 4.45 (s, 6H, -PTA), 3.83 (s, 6H, -PTA), 2.56 (s, 6H, 4,4′-2xCH_3); ^{13}C NMR (151 MHz, $CDCl_3$), δ (ppm): 193.0, 187.4,155.5, 154.2, 152.22, 129.2, 127.3, 73.6, 73.5, 72.8, 72.7, 56.3, 55.9, 50.5, 50.3, 49.7, 49.6, 21.9; ^{31}P NMR (400 MHz, $CDCl_3$), δ (ppm): −79.3; IR (KBr, cm^{-1}), ν_{CO}: 2029, 1914; UV/Vis, λ^{max}, nm (ε, M^{-1} cm^{-1}): 361 (2810); Anal. Calc. for $C_{21}H_{27}N_6O_6PRe$: C, 37.28; H, 4.02; N, 12.42; Found: C, 37.25; H, 4.00; N, 12.40 %.

*fac-[Re(CO)$_3$(4,4′-DiMBpy)(CyPh$_2$P)][NO$_3$] (**9**)*. Yield: 30 mg, 77.83 %; ^{1}H NMR (400 MHz, $CDCl_3$), δ (ppm): 8.96–8.95 (d, $J = 6$ Hz, 2H, H6/6′), 7.99 (s, 2H, H3/3′), 7.54–7.469 (m, 10*H*, -Ph_2P), 7.39–7.37 (dd, $J = 1$ Hz, $J = 6$ Hz, 2H, H5/5′), 2.60 (s, 6H, 4,4′-2xCH_3), 2.30–2.19 (m, 1H, -CyP), 1.83–1.73 (m, 5H, -CyP), 1.34–1.24 (m, 5H, -CyP); ^{13}C NMR (151 MHz, $CDCl_3$), δ (ppm): 196.7, 193.6, 155.7, 155.5, 153.5, 152.6, 152.2, 151.3, 131.1, 131.1, 128.6, 128.5, 124.1, 37.5, 37.0, 29.7, 29.3, 26.4, 26.4, 25.8, 24.8, 24.8, 22.1, 21.9; ^{31}P NMR (400 MHz, $CDCl_3$), δ (ppm): 34.3; IR (KBr, cm^{-1}), ν_{CO}: 2022, 1981; UV/Vis, λ^{max}, nm (ε, M^{-1} cm^{-1}): 355 (4572); Anal. Calc. for $C_{33}H_{36}N_3O_6PRe$: C, 50.31; H, 4.61; N, 5.33; Found: C, 50.28; H, 4.59; N, 5.31 %.

*fac-[Re(CO)$_3$(4,4′-DiMBpy)(Cy$_2$PhP)][NO$_3$] (**10**)*. Yield: 31 mg, 80.75 %; ^{1}H NMR (400 MHz, $CDCl_3$), δ (ppm): 8.96–8.94 (d, $J = 6$ Hz, 2H, H6/6′), 7.99 (s 2H, H3/3′), 7.69–7.64 (m, 3H, -PhP), 7.57–7.52 (m, 2H, -PhP), 7.39–7.37 (dd, $J = 1$ Hz, $J = 6$ Hz, 2H, H5/5′), 2.60 (s, 6H, 4,4′-2xCH_3), 2.19–2.12 (m, 2H, -Cy_2P), 1.86–1.64 (m, 10*H*, -Cy_2P), 1.38–1.15 (m, 10*H*, -Cy_2P); ^{13}C NMR (151 MHz, $CDCl_3$), δ (ppm): 152.6, 151.3, 131.6, 131.5, 131.4, 128.5, 128.4, 128.2, 128.0, 124.1, 35.2, 34.5, 26.5, 26.3, 26.2, 25.8, 25.4, 24.5, 21.9; ^{31}P NMR (400 MHz, $CDCl_3$), δ (ppm): 60.5; IR (KBr, cm^{-1}), ν_{CO}: 2026, 1900; UV/Vis, λ^{max}, nm (ε, M^{-1} cm^{-1}): 354 (4147); Anal. Calc. for $C_{33}H_{42}N_3O_6PRe$: C, 49.93; H, 3.21; N, 5.29; Found: C, 49.96; H, 5.30; N, 5.27 %.

*fac-[Re(CO)$_3$(5,5′-DiMBpy)(PPh$_3$)][NO$_3$] (**11**)*. Yield: 31 mg, 83.33 %; ^{1}H NMR (400 MHz, $CDCl_3$), δ (ppm): 8.93–8.91 (d, $J = 7$ Hz, 2H, H6/6′), 7.99 (s, 2H, H3/3′), 7.72–7.66 (m, 6H, -PPh_3), 7.59–7.55 (t, $J = 7$ Hz, 3H, -PPh_3), 7.51–7.46 (ddd, $J = 3$ Hz, $J = 3$ Hz, $J = 3$ Hz, 6H, -PPh_3), 7.40–7.40 (d, $J = 5$ Hz, 2H, H4/4′), 2.19 (s, 6H, 5,5′-2xCH_3); ^{13}C NMR (151 MHz, $CDCl_3$), δ (ppm): 153.2, 152.3, 139.5, 137.7, 132.9, 132.8, 132.8, 131.8, 130.9, 129.4, 129.3, 122.3, 18.7, 18.6; ^{31}P NMR (400 MHz, $CDCl_3$), δ (ppm): 29.1; IR (KBr, cm^{-1}), ν_{CO}: 2022, 1902; UV/Vis, λ^{max}, nm (ε, M^{-1} cm^{-1}): 350 (3873); Anal. Calc. for $C_{33}H_{30}N_3O_6PRe$: C, 50.70; H, 3.87; N, 5.37; Found: C, 50.68; H, 3.88; N, 5.39 %.

*fac-[Re(CO)$_3$(5,5′-DiMBpy)(PTA)][NO$_3$] (**12**)*. Yield: 25 mg, 77.21 %; ^{1}H NMR (400 MHz, $CDCl_3$), δ (ppm): 8.82 (s, 2H, H6/6′), 8.71–8.69 (d, $J = 6$ Hz, 2H, H3/3′), 7.44–7.42 (d, $J = 6$ Hz, 2H, H4/4′), 4.48–4.39 (q, $J = 11$ Hz, 6H, -PTA), 3.81 (s, 6H, -PTA), 2.73 (s, 6H, 5,5′-2xCH_3); ^{13}C NMR (151 MHz, $CDCl_3$), δ (ppm): 153.8, 153.6, 152.2, 149.5, 141.6, 138.9, 137.4, 133.0, 125.5, 120.3, 73.6, 73.6, 72.5, 72.4, 56.3, 55.8,

50.6, 50.4, 49.6, 49.4, 18.6, 18.3; ^{31}P NMR (400 MHz, $CDCl_3$), δ (ppm): −79.3; IR (KBr, cm^{-1}), ν_{CO}: 2020, 1905; UV/Vis, λ^{max}, nm (ε, M^{-1} cm^{-1}): 355 (2874); Anal. Calc. for $C_{21}H_{27}N_6O_6PRe$: C, 37.28; H, 4.02; N, 12.42; Found: C, 37.29; H, 3.99; N, 12.44 %.

fac-[Re(CO)$_3$(5,5′-DiMBpy)(CyPh$_2$P)][NO$_3$] ***(13)***. Yield: 31 mg, 79.66 %; ^{1}H NMR (400 MHz, $CDCl_3$), δ (ppm): 8.50–8.49 (dd, $J = 1$ Hz, $J = 2$ Hz, 2H, H6/6′), 8.26–8.24 (d, H = 8 Hz, 2H, H3/3′), 7.63–7.60 (dd, $J = 2$ Hz, $J = 8$ Hz, 2H, H4/4′), 7.49–7.47 (m, 5H, -Ph$_2$P), 7.33–7.32 (m, 5H, -Ph$_2$P), 2.39 (s, 6H, 5,5′-2xCH$_3$), 2.26–2.18 (m, 1H, -CyP), 1.97–1.55 (m, 10*H*, -CyP); ^{13}C NMR (151 MHz, $CDCl_3$), δ (ppm): 153.8, 153.1, 153.0,149.5, 141.2, 139.6, 137.4, 133.7, 131.5, 131.1, 131.0, 128.8, 128.6, 128.6, 128.5, 128.3,128.2, 125.7, 125.6, 125.3, 120.3, 37.5, 29.7, 29.5, 24.8, 24.8, 18.6, 18.5, 18.3; ^{31}P NMR (400 MHz, $CDCl_3$), δ (ppm): 34.5; IR (KBr, cm^{-1}), ν_{CO}: 2022, 1899; UV/Vis, λ^{max}, nm (ε, M^{-1} cm^{-1}): 356 (3884); Anal. Calc. for $C_{33}H_{36}N_3O_6PRe$: C, 50.31; H, 4.61; N, 5.33; Found: C, 50.30; H, 4.63; N, 5.30 %.

fac-[Re(CO)$_3$(5,5′-DiMBpy)(Cy$_2$PhP)][NO$_3$] ***(14)***. Yield: 50 mg, 78.95 %; ^{1}H NMR (400 MHz, $CDCl_3$), δ (ppm): 8.51–8.50 (dd, $J = 1$ Hz, $J = 2$ Hz, 2H, H6/6′), 8.28–8.26 (d, $J = 8$ Hz, 2H, H3/3′), 7.70–7.64 (m, 2H, H4/4′), 7.63–7.62 (dd, $J = 1$ Hz, $J = 2$ Hz, 5H, -PhP), 2.40 (s, 6H, 5,5′-2xCH$_3$), 2.06–2.04 (m, 1H, -Cy$_2$P), 1.95–1.74 (m, 11*H*, -Cy$_2$P), 1.70–1.59 (m, 10*H*, -Cy$_2$P); ^{13}C NMR (151 MHz, $CDCl_3$), δ (ppm): 153.8, 149.5, 137.4, 134.8, 134.6, 133.0, 131.5, 131.4, 128.3, 128.2, 120.3, 35.5, 34.8, 32.5, 32.4, 30.1, 30.0, 28.8, 28.8, 26.4, 18.3; ^{31}P NMR (400 MHz, $CDCl_3$), δ (ppm): 51.1; IR (KBr, cm^{-1}), ν_{CO}: 2023, 1901; UV/Vis, λ^{max}, nm (ε, M^{-1} cm^{-1}): 352 (3915); Anal. Calc. for $C_{33}H_{42}N_3O_6PRe$: C, 49.93; H, 5.33; N, 5.29; Found: C, 49.91; H, 5.31; N, 5.25 %.

fac-[Re(CO)$_3$(4,4′-DiMoxBpy)(PPh$_3$)][NO$_3$] ***(15)***. Yield: 34 mg, 75.89 %; ^{1}H NMR (300 MHz, $CDCl_3$), δ (ppm): 8.88–8.86 (d, $J = 6$ Hz, 2H, H6/6′), 8.06–8.05 (d, $J = 6$ Hz, 2H, H3/3′), 7.51–7.46 (m, 12H, -PPh$_3$), 7.41–7.39 (m, 3H, -PPh$_3$), 7.02–6.99 (dd, $J = 3$ Hz, $J = 3$ Hz, 2H, H5/5′), 4.29 (s, 6H, 4,4′-2xOCH$_3$); ^{13}C NMR (151 MHz, $CDCl_3$), δ (ppm): 168.9, 158.3, 154.4, 152.4, 133.0, 132.9, 132.2, 132.1, 129.3, 129.2, 128.6, 128.5, 116.6, 113.5, 110.7, 58.1; ^{31}P NMR (400 MHz, $CDCl_3$), δ (ppm): 29.1; IR (KBr, cm^{-1}), ν_{CO}: 2027, 1911; UV/Vis, λ^{max}, nm (ε, M^{-1} cm^{-1}): 354 (3964); Anal. Calc. for $C_{33}H_{30}N_3O_8PRe$: C, 48.70; H, 3.72; N, 5.16; Found: C, 48.72; H, 3.70; N, 5.14 %.

fac-[Re(CO)$_3$(4,4′-DiMoxBpy)(PTA)][NO$_3$] ***(16)***. Yield: 50 mg, 78.90 %; ^{1}H NMR (400 MHz, $CDCl_3$), δ (ppm): 8.49–8.47 (d, $J = 5$ Hz, 2H, H6/6′), 7.99–7.98 (d, $J = 3$ Hz, 2H, H3/3′), 6.87–6.85 (dd, $J = 3$ Hz, $J = 6$ Hz, 2H, H5/5′), 4.63 (s, 6H, -PTA), 4.08–4.06 (d, $J = 10$ Hz, 6H, -PTA), 3.96 (s, 6H, 4,4′-2xOCH$_3$); ^{13}C NMR (151 MHz, $CDCl_3$), δ (ppm): 166.7, 157.9, 150.1, 111.1, 106.2, 73.5, 73.5, 72.4, 72.3, 55.3, 50.4, 50.2; ^{31}P NMR (400 MHz, $CDCl_3$). δ (ppm): −77.8; IR (KBr, cm^{-1}), ν_{CO}: 2026, 1908; UV/Vis, λ^{max}, nm (ε, M^{-1} cm^{-1}): 352 (1962); Anal. Calc. for $C_{21}H_{27}N_6O_8PRe$: C, 35.59; H, 3.84; N, 11.86; Found: C, 35.55; H, 3.82; N, 11.84 %.

fac-[Re(CO)$_3$(4,4′-DiMoxBpy)(CyPh$_2$P)][NO$_3$] ***(17)***. Yield: 34 mg, 75.63 %; ^{1}H NMR (400 MHz, $CDCl_3$), δ (ppm): 8.91–8.89 (d, $J = 6$ Hz, 2H, H6/6′), 8.18–8.17 (d, $J = 6$ Hz, 2H, H3/3′), 7.83–7.78 (m, 2H, -Ph$_2$P), 7.51–7.48 (m, 7H, -Ph$_2$P), 7.42–7.40 (m, 3H, -Ph$_2$P), 7.02–7.00 (dd, $J = 3$ Hz, $J = 3$ Hz, 2H, H5/5′), 4.26 (s, 6H, 4,4′-2xOCH$_3$), 2.30–2.21 (m, 1H, -CyP), 1.83–1.82 (m, 2H, -CyP), 1.73–1.71 (m, 8H, -CyP); ^{13}C NMR (151 MHz, $CDCl_3$), δ (ppm): 168.8, 158.2, 152.7, 133.8, 133.7, 131.7, 131.2, 131.1, 129.5, 129.4, 128.8, 128.6, 116.8, 27.8, 26.4, 26.3, 25.7, 24.7; ^{31}P NMR (400 MHz, $CDCl_3$), δ (ppm): 34.3; IR (KBr, cm^{-1}), ν_{CO}: 2026, 1905; UV/Vis, λ^{max}, nm (ε, M^{-1} cm^{-1}): 349 (3596); Anal. Calc. for $C_{33}H_{36}N_3O_8PRe$: C, 48.35; H, 4.43; N, 5.13; Found: C, 48.33; H, 4.40; N, 5.10 %.

fac-[Re(CO)$_3$(4,4′-DiMoxBpy)(Cy$_2$PhP)][NO$_3$] ***(18)***. Yield: 35 mg, 78.01 %; ^{1}H NMR (400 MHz, $CDCl_3$), δ (ppm): 8.50–8.48 (d, $J = 6$ Hz, 2H, H6/6′), 8.02–8.01 (d, $J = 3$ Hz, 2H, H3/3′), 7.71–7.65 (m, 1H, -PhP), 7.54–7.45 (m, 3H, -PhP), 7.35–7.33 (m, 1H, -PhP), 6.89–6.87 (dd, $J = 3$ Hz, $J = 6$ Hz, 2H, H5/5′), 3.97 (s, 6H, 4,4′-2xOCH$_3$), 2.08–2.02 (m, 1H, -Cy$_2$P), 1.95–1.76 (m, 11*H*, -Cy$_2$P), 1.69–1.60 (m, 10*H*, -Cy$_2$P); ^{13}C NMR (151 MHz, $CDCl_3$), δ (ppm): 166.7, 175.9, 154.0, 150.1, 131.5, 131.4, 128.3, 128.2, 111.1, 106.2, 55.3, 35.5, 34.8, 26.4, 25.9, 25.8; ^{31}P NMR (400 MHz, $CDCl_3$), δ (ppm): 59.8; IR (KBr, cm^{-1}), ν_{CO}: 2023, 1897; UV/Vis, λ^{max}, nm (ε, M^{-1} cm^{-1}): 357 (3777); Anal. Calc. for $C_{33}H_{42}N_3O_8PRe$: C, 47.99; H, 5.13; N, 5.09; Found: C, 48.00; H, 5.10; N, 5.07 %.

2.3. Single-crystal X-ray crystallography

The crystal structure data of **2a, 3a** and **4** were collected on a Bruker D8 Quest Eco Chi Photon II CPAD diffractometer. All the cell refinements and data reduction were completed using SAINT-Plus and XPREP [24]. To correct the absorption effects, the multi-scan technique and software package SADABS [31] were used. All the crystal structures were solved using the direct method package SIR-97 [25] and refined by using WinGX [26] and SHELXL-97 [27]. The crystal structures' graphical representation was obtained with the program DIAMOND [28]. The structures are shown with thermal ellipsoids drawn at the 50 % probability level, unless otherwise stated. A summary of the general crystal data and refinement parameters for complexes **2a, 3a** and **4** are given in Table SI 1 (†ESI).

2.4. UV/Vis absorbance and photoluminescence

The UV/Vis absorbance measurement was conducted in a 1 cm tandem quartz cuvette on a Varian Cary 50 Conc. spectrophotometer. All

Table 1
A summary of the IR stretching frequencies, UV/Vis and ^{31}P NMR data of complexes **1**–**18**.

Complex	IR (cm^{-1})	UV/Vis (nm)	ε (M^{-1} cm^{-1})	^{31}P (δ, ppm)
***fac*-[Re(CO)$_3$(4,4′-DiMBpy)(H$_2$O)]$^+$ (1)**	2023, 1914, 1868	360	(3 680)	–
***fac*-[Re(CO)$_3$(5,5′-DiMBpy)(H$_2$O)]$^+$ (2)**	2017, 1888	355	(3 235)	–
***fac*-[Re(CO)$_3$(4,4′-DiMoxBpy)(H$_2$O)]$^+$ (3)**	2021, 1879	350	(4 720)	–
***fac*-[Re(CO)$_3$(4,4′-DiMBpy)(Br)] (4)**	2013, 1881, 1864	380	(3 685)	–
***fac*-[Re(CO)$_3$(5,5′-DiMBpy)(Br)] (5)**	2018, 1934, 1897	375	(2 925)	–
***fac*-[Re(CO)$_3$(4,4′-DiMoxBpy)(Br)] (6)**	2024, 1886	365	(3 995)	–
***fac*-[Re(CO)$_3$(4,4′-DiMBpy)(PPh$_3$)]$^+$ (7)**	2025, 1909	347	(3 860)	29.13
***fac*-[Re(CO)$_3$(4,4′-DiMBpy)(PTA)]$^+$ (8)**	2029, 1914	361	(2 810)	−79.26
***fac*-[Re(CO)$_3$(4,4′-DiMBpy)(CyPh$_2$P)]$^+$ (9)**	2026, 1900	354	(4 147)	60.64
***fac*-[Re(CO)$_3$(4,4′-DiMBpy)(Cy$_2$PhP)]$^+$ (10)**	2022, 1981	355	(4 572)	34.26
***fac*-[Re(CO)$_3$(5,5′-DiMBpy)(PPh$_3$)]$^+$ (11)**	2022, 1902	350	(3 873)	29.13
***fac*-[Re(CO)$_3$(5,5′-DiMBpy)(PTA)]$^+$ (12)**	2020, 1905	355	(2 874)	−79.31
***fac*-[Re(CO)$_3$(5,5′-DiMBpy)(CyPh$_2$P)]$^+$ (13)**	2022, 1898	352	(3 915)	51.14
***fac*-[Re(CO)$_3$(5,5′-DiMBpy)(Cy$_2$PhP)]$^+$ (14)**	2023, 1901	356	(3 884)	34.53
***fac*-[Re(CO)$_3$(4,4′-DiMoxBpy)(PPh$_3$)]$^+$ (15)**	2027, 1911	354	(3 964)	29.08
***fac*-[Re(CO)$_3$(4,4′-DiMoxBpy)(PTA)]$^+$ (16)**	2026, 1908	352	(1 962)	−77.76
***fac*-[Re(CO)$_3$(4,4′-DiMoxBpy)(CyPh$_2$P)]$^+$ (17)**	2023, 1897	349	(3 777)	59.84
***fac*-[Re(CO)$_3$(4,4′-DiMoxBpy)(Cy$_2$PhP)]$^+$ (18)**	2026, 1905	357	(3 596)	34.32

the UV/Vis data of the complexes are reported in Table 1, with the maximum wavelength and the absorptivity coefficient; GC-acetone was used as the solvent. Furthermore, the same samples for UV/Vis absorption were utilized for the photoluminescence analysis.

2.5. Photoluminescence studies

An Edinburgh Instruments FLS980 machine with a 450 W xenon lamp steady-state excitation source was used to measure the photoluminescence emission and excitation spectra. Quantum yields were then measured near the maximum excitation wavelength using an integrating sphere accessory by dividing the luminescence output (i.e. integrated area under the emission curve) by the absorbed light (i.e. integrated difference of the sample and pure solvent near the excitation wavelength). A neutral density filter was applied when measuring the absorbed light and compensated for using its measured transmission curve.

2.6. Biological studies

2.6.1. Cell culture

The human breast adenocarcinoma MDA-MB-231 (triple-negative) and MCF-7 (estrogen receptor-positive) cells were maintained in DMEM (Highveld Biologicals, Lyndhurst, United Kingdom (UK) and RPMI 1640 (Highveld Biologicals, Lyndhurst, United Kingdom (UK) respectively, supplemented with 10 % Fetal Bovine Serum (FBS) and 100 U/ml penicillin and 100 μg/ml streptomycin. The MRC-5 human lung fibroblasts were cultured in DMEM supplemented with 20 % FBS and 100 U/ml penicillin and 100 μg/ml streptomycin. When treated with the test compounds, the MRC-5 cells were cultured in DMEM medium supplemented with 10 % FBS. All cells were maintained at 37 °C in a 5 % CO_2–95 % air-humidified incubator.

2.6.2. Cell treatments

The compounds were dissolved in dimethyl sulfoxide (DMSO) (Merck 48856212719) to achieve a final stock concentration of 5 mM, heated at 100° C for 2 min and then stored at room temperature for a maximum of 5 days before use. The 5 mM stock solutions were further diluted using cell culture medium to attain final experimental concentrations of 10 μM and a vehicle control (DMSO) of the equivalent highest compound concentration was prepared simultaneously. Cisplatin (Pfizer ltd, New York, USA) was used as the positive control at its reported IC_{50} values for MCF-7, MDA-MB-231 and MRC-5 cells.

2.6.3. Cytotoxicity assay

The MCF-7 and MDA-MB-231 breast cancer cells, along with MRC-5 fibroblasts, were plated in 96-well plates and treated with a concentration of 10 μM of the compounds or vehicle (DMSO) for a period of 48 h. The cytotoxicities of these compounds were evaluated using a 3-(4,5 dimethylthiazol-2-yl)-2,5-diphenyltrazolium bromide (MTT) assay (M21281G, Sigma-Aldrich), according to the manufacturer's instructions. The mean cell viability was calculated as a percentage of the mean of the vehicle control. At least two independent experiments in quadruplicate were performed, from which the half maximal inhibitory concentration (IC_{50}) was determined using graph prism version 6.0. The selectivity index (SI) was calculated using the following formula (IC_{50} for normal MRC-5 fibroblasts) / (IC_{50} for breast cancer cell line).

3. Results and discussion

Synthesis and Characterisation: This study reports on the synthesis and spectroscopic characterisation of eighteen Re(I) tricarbonyl complexes (**1**–**18**). Initially, the rhenium precursor *fac*-$[NEt_4]_2[Re(CO)_3(Br)_3]$ was dissolved in H_2O at an adjusted pH of 2.2 to prevent the formation of a polymeric species in the solution. This was followed by the addition of three equivalents of $AgNO_3$ to remove all the bromide ligands for the successful synthesis of the *fac*-$[Re(CO)_3(H_2O)_3]^+$ intermediate. Most of the synthesized complexes formed yellow to orange precipitates in moderate to high yields (60–85 % yield). The aqua (**1**–**3**) and bromide coordinated Re(I) complexes (**4**–**6**) had lower yields because some complexes dissolved when the precipitates were washed with cold ethanol. Two moles of the *N,N′*-bid ligands were reacted with one mole of *fac*-$[NEt_4]_2[Re(CO)_3(Br)_3]$, and an increase in the reflux temperature to 50 ℃ was required to increase the yields of **1**–**3** and **4**–**6**. The aqua complexes (**1**–**3**) dissolved almost immediately after being washed with cold ethanol and afforded crystals of *fac*-$[Re(CO)_3$(5,5′-DiMBpy)$(NO_3)]$ (**2a**) and *fac*-$[Re(CO)_3$(4,4′-DiMoxBpy)$(NO_3)]$ $[(CH_3)_2CO]$ (**3a**) from the filtrates of **2** and **3**, respectively. The precipitates of all the complexes were dried and recrystallized with a solvent mixture of hexane:DCM (1:1), which afforded the molecular structure of *fac*-$[Re(CO)_3$(4,4′-DiMBpy)(Br)] (**4**). What is notable is that complexes **2a** and **3a** were obtained from the somewhat solvent-contaminated filtrates of the mother complexes. Furthermore, the successful syntheses of complexes **1**–**3** required more effort. The synthesis of complexes **7** to **18** was conducted through the substitution of the aqua ligand in *fac*-$[Re(CO)_3$(*N,N′*-bid)$(H_2O)]^+$ by different monodentate phosphines (PPh_3, PTA, $CyPh_2P$, Cy_2PhP) via the '2 + 1' approach. *fac*-$[Re(CO)_3$(*N,N′*-bid)$(H_2O)]^+$ was dissolved in methanol at 80 C before the addition of the different monodentate phosphines, then the reaction mixture was refluxed for 48 h to afford the desired product. Full characterization of these complexes was done using IR, NMR and UV/Vis characterization methods.

The Re(I) tricarbonyl complexes reported in this study have a d^6 configuration and their lowest excited state usually is metal-to-ligand charge transfer (MLCT) in character. There is a broad range in the determined molar absorptivity (ε) observed for complexes **1**–**18**, which differ between 1962 and 4720 M^{-1} cm^{-1}, and compare well with similar structures [29–31].

The carbonyl stretching frequencies of the Re(I) complexes **1**–**18** are pretty similar and are comparable to reported similar structures, consisting of values ranging from 2029 to 1864 cm^{-1} [32,33]. Complexes **4**–**6**, with the coordinated bromide ligand, are found to have stretching frequencies in the range 2013 to 2024 cm^{-1}, with complex **6** at the higher stretching frequency, possibly due to the coordinated methoxy group on the chelating bidentate ligand.

There is an increase in the carbonyl band ranges for the phosphine coordinated complexes **7**–**18**; this is particularly evident in the triphenylphosphine containing complexes (**11** < **7** < **15**). Even though there are outliers in the IR data obtained for the phosphine coordinated complexes, a noticeable trend was observed in the ^{31}P shifts, showing the following electron donating effect: PTA > PPh_3 > Cy_2PhP > $CyPh_2P$. In the 5,5′-DiMBpy and 4,4′-DiMoxBpy coordinated complexes, the IR frequency differences are small, however there are noticeable differences in the IR carbonyl stretching frequencies of the 4,4′-DiMBpy coordinated complexes with different monodentate ligands.

All the NMR spectra were obtained from the solvents as stated in the procedure. The ^1H and ^{13}C NMR data obtained for the synthesized complexes are consistent with the proposed structures and existing literature data for some of the complexes. In the coordinated state of the 4,4′-DiMBpy, 5,5′-DiMBpy and 4,4′-DiMoxBpy ligands, characteristic shifts are prominent compared to their non-coordinated states. Additionally, as expected, the methoxy group (in 4,4′-DiMoxBpy) was more upfield than the methyl group (in 4,4′-DiMBpy) due to the attached oxygen atom [34]. Furthermore, for most complexes, the CO signals were not detected, because it required the samples to be run for longer periods on the NMR instrument. The ^{31}P NMR data of complexes **7**–**18** were obtained, displaying a single peak, as illustrated in Table 1, proving the absence of isomers. These complexes also show significant downfield shifts compared to the free phosphine ligands, confirming the formation of a Re-P bond. During the phosphine complexes' initial synthesis, some of the mono-phosphine ligands were oxidized. Therefore, to overcome the oxidation of the phosphine ligands, the reagent

bottles were sealed and stored in a desiccator. Additionally, 85 % phosphoric acid was used as a reference to prevent sidebands that might occur for the ^{31}P NMR spectra [35]. In the PTA coordinated complexes **8**, **12** and **16**, the significant donating ability of the PTA ligand is observed, with upfield shifts of δ −79.26, −79.31 and −77.76 ppm respectively. A downfield ^{31}P NMR shift was noted for **7**, **9**, **10**, **11**, **13**, **14**, **15**, **17** and **18**, displaying the electron withdrawing effect of the $CyPh_2P$ ligand, as the $CyPh_2P$ coordinated complexes appeared more downfield (at δ 60.64, 51.14 and 59.84 ppm for **9**, **13** and **17**). A trend can be deduced from the phosphine coordinated ligands in terms of their electron withdrawing nature, as observed in the ^{31}P NMR, with the following decreasing arrangement: $CyPh_2P$ > Cy_2PhP > PPh_3, which correlates well with similar studies [22,23,36].

X-ray crystallography: The crystal structures of *fac*-[Re(CO)$_3$(5,5′-DiMBpy)(NO$_3$)] (**2a**), *fac*-[Re(CO)$_3$(4,4′-DiMoxBpy)(NO$_3$)][(CH$_3$)$_2$CO] (**3a**) and *fac*-[Re(CO)$_3$(4,4′-DiMBpy)Br] (**4**) were obtained from the slow evaporation of the solvents, as described in the experimental section. The crystal data of **2a**, **3a** and **4** are presented in Table SI 1 (†ESI) and the molecular diagrams illustrating the numbering scheme are given in Fig. 1.

Literature and crystal structures involving Re(I) tricarbonyl complexes have been intensively studied [37–40]. **2a** crystallized in the triclinic crystal system, in the $P\bar{1}$ space group, with two molecules in the unit cell (Z = 2), **3a** in the monoclinic crystal system, in the $C2/c$ space group, with eight molecules in the unit cell (Z = 8) and finally **4** in the monoclinic crystal system, $P2_1/c$ space group, with Z = 4. A summary of the bond distances and angles for **2a**, **3a**, and **4** are presented in Table SI 2 (†ESI) for the sake of comparison.

The complexes **2a**, **3a** and **4** have a rhenium metal center covalently bonded to three facially orientated carbonyl ligands with a chelate *N,N′*-bidentate ligand (4,4-DiMBpy for **4**, 5,5′-DiMBpy for **2a** and 4,4′-DiMoxBpy for **3a**), and either a nitrate (**2a** and **3a**) or a bromide (**4**) substituent in the 6th position. Furthermore, the rhenium to carbon bond distances range from 1.893 to 1.926 Å, and the rhenium to nitrogen bond distances from 2.169(4) to 2.175(6) Å. The bond distances from the rhenium atom to the axial position substituent for **2a** (Re01-O4) is 2.152(5) Å, **3a** (Re01-O4) is 2.156(3) Å and **4** (Re1-Br1) is 2.631 (7), as summarised in Table SI 2 (†ESI), which are considered to be within the normal range [41–44].

Octahedral distortion was noted in all the complexes by the deviation of the bond angles from the ideal value of 180°, with the following angles in **2a** and **3a** (O4-Re1-C1) of 171.40(2) ° and 173.72(15) °, respectively, and in **4** (Br1-Re1-C1) of 177.57(14) °. The ligand bite angles (N1-Re1-N2) for **2a** (74.80(2) °), **3a** (74.57(13) °) and **4** (74.74 (15) °) are within the same range and correlate well with similar structures [45–52]. This study also reports on the type of geometries found with regards to the π···π interactions that were identified in the reported solid-state structures (†ESI, Figure SI 1). This information is essential since it provides a basic understanding of drug-drug interactions and is critical in determining the structural and molecular recognition properties in biological studies, such as proteins, nucleic acids and peptides [53]. Literature reports by Walters (2002) [53], Zhao *et al.* (2015) [54] and Wolff *et al.* (2013) [55] were used to determine the geometry. There are three primary geometries of aromatic interactions, namely edge-face (4.96–5.025 Å), offset stacked (3.4–3.6 Å) and face-to-face stacked (3.3–3.8 Å); however, the offset stacked confirmation is the ideal geometry [54]. The only structure that had π···π interactions worth noting, based on the criteria reported in the literature, is **2a**, with a face-to-face stacked geometry (3.730(10) Å).

Photoluminescence studies: The focus of numerous researchers is on a vital class of complexes of the form: *fac*-[Re(CO)$_3$(*N,N′*)(X)], where *N, N′* = diimine and X = halides, and these complexes produce remarkable phosphorescent characteristics [56–58]. This study involves aqua, bromide and phosphorous coordinated Re(I) complexes. To confirm the suitability for the synthesized complexes as PDT and MI agents, a solution state luminescence study was performed on all the synthesized complexes **1**–**18** and the results are compared with the literature on different *N,N′*-donor coordinated complexes. Fig. 2 below, shows the combined excitation and emission spectra of all the complexes, whereas Table 2 summarizes the UV/Vis excitation wavelengths, emission wavelengths, stokes shifts and the quantum yield data of the respective complexes.

The complexes display characteristic broad emission peaks ranging from 545 to 620 nm, with a slightly broad excitation range of 347 to 380 nm. The difference in the observed excitation wavelengths is induced by the nature of the bidentate ligand used and/or the coordinated monodentate ligands in the sixth position (*see* Scheme 1). The complexes **8**, **12** and **16** are evident to the latter statement, exhibiting PTA coordinated complexes having untraceable emission properties within the range. Seldomly observed, ligands infested with C—H bonds, which are known for promoting effective thermal relaxations from the excited state often leading to quenched luminescence, are of no surprise with low complex quantum yields [74,75]. The notable, ≤5 nm, difference in the absorption nature amongst these complexes leads to *ca.* a 60 nm deviation of the stoke shifts, as illustrated in Table 2. Contrary to common observed behavior [30], we herein have noticeable hypsochromic shifts for all the PR_3 coordinated complexes as compared to the aqua and bromido coordinated complexes **1**–**6**.

Tsubaki and co-workers reported that PR_3 derivatives with trialkyl or triaryl substituents allow intramolecular interactions with the Bp bidentate ligand [76], promoting bathochromic shifts, which is completely contrary to the phenyl and cyclohexyl PR_3 ligands, which arguably act as spacers, forbidding any intra-ligand interactions in this work. Moreover, complexes **1** and **4** record the highest stoke shifts of 260 and 270 nm in the range, with the lowest being 200 and 196 nm from complexes **15** and **17**. The low stokes shifts were evidently due to the observed 55 nm blue-shifted emission wavelengths for complexes **15** and **17**, respectively, as observed in Fig. 2. Interestingly, complexes **5**,

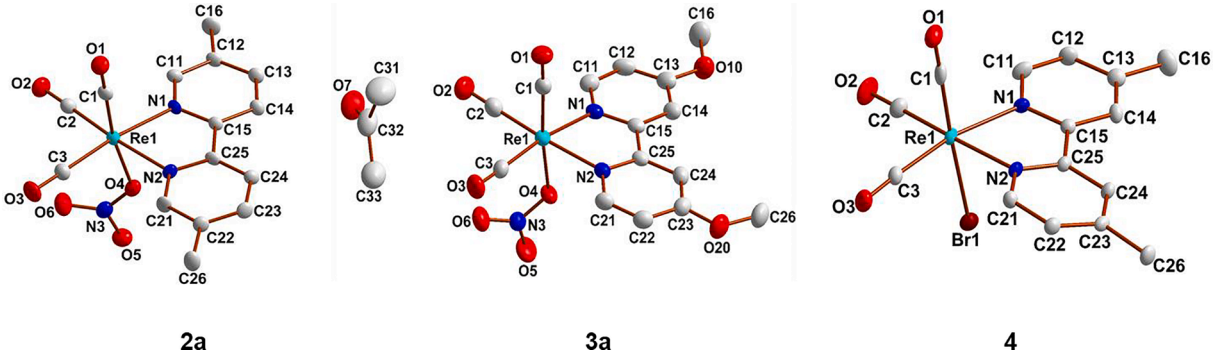

Fig. 1. Molecular representation of the crystal structures of *fac*-[Re(CO)$_3$(5,5′-DiMBpy)(NO$_3$)] (**2a**), *fac*-[Re(CO)$_3$(4,4′-DiMoxBpy)(NO$_3$)][(CH$_3$)$_2$CO] (**3a**) and *fac*-[Re(CO)$_3$(4,4′-DiMBpy)(Br)] (**4**). Hydrogen atoms and numbering for certain atoms are omitted for clarity.

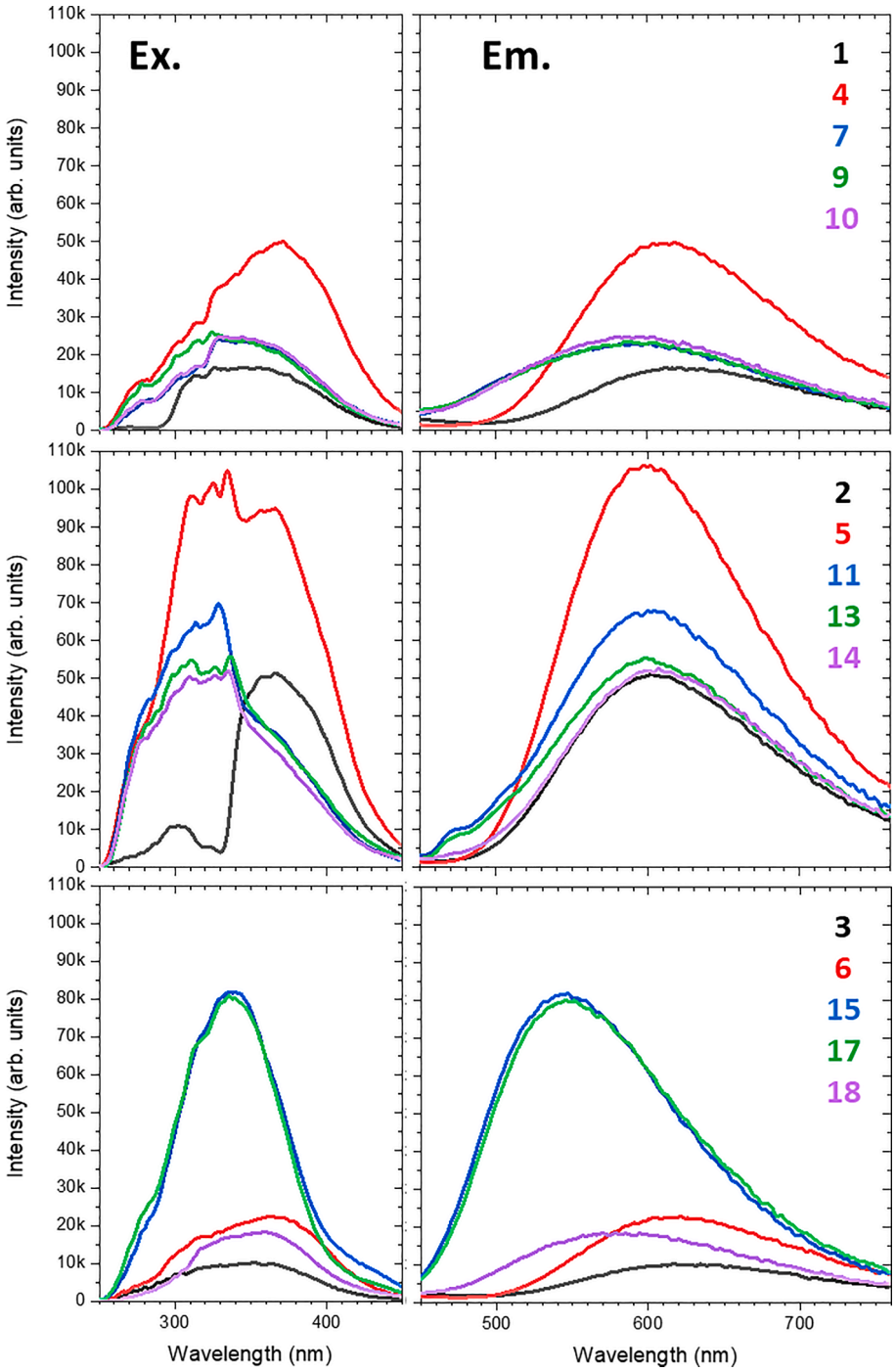

Fig. 2. An illustration of the combined excitation and emission spectra of the complexes **1–18**.

11, **15** and **17** proved to have the highest quantum yields and that correlates quite well with the results obtained from the literature [34,59–66].

It is further worth noticing an overarching observation in the quantum yields of the complexes with the various *N,N′*-donor coordinated ligands: 4,4′-DiMBpy < 4,4′-DiMoxBpy < 5,5′-DiMBpy with respective coordinated monodentate ligands (aqua, PR_3 and bromide). 4,4′-DiMBpy < 5,5′-DiMBpy in the comparisons is likely due to the relative inductive effect of the electron-donating groups attached to Bp-ligands in synergy with the electron-withdrawing effect of not only the aqua and bromide but also the PR_3 monodentate ligands, leading to MLCT excited states.

Biological studies: An *in vitro* biological cell study was conducted on all the synthesized complexes to determine their activity and cytotoxicity towards female-related cancerous cells, MCF-7, and triple-negative breast cancer cell lines, MDA-MB-231. This study was motivated by numerous literature reports on Re(I) tricarbonyl complexes that display cytotoxicity against breast cancer cell lines [60,67–77]. The results from this study are illustrated in Figure SI 2 (†ESI), and the data are summarised in Table 3. The values in Table 3 are the averages of two independent experiments, each performed in quadruplicate.

After a preliminary study, that involved the determination of moderate activity among the 18 complexes, it was determined that only **6** and **13** showed considerable cytotoxicity. Furthermore, the stability of **6** and **13** was determined in DMSO at 100 °C, and the NMR results confirmed that the complexes were stable under these conditions. **6**

Table 2
A summary of the photophysical properties for the synthesized complexes **1**–**18**, compared with results obtained from previous studies.

Compounds	UV/Vis, nm	Excitation, nm	Emission, nm	Stokes shift		Quantum yield (%)
				nm	cm^{-1} *	
***fac*-[Re(CO)$_3$(4,4′-DiMBpy)(H$_2$O)]$^+$ (1)**	360	350	620	260	11,649	0.27
***fac*-[Re(CO)$_3$(5,5′-DiMBpy)(H$_2$O)]$^+$ (2)**	355	365	605	250	11,640	0.71
***fac*-[Re(CO)$_3$(4,4′-DiMoxBpy)(H$_2$O)]$^+$ (3)**	350	350	620	270	12,442	0.15
***fac*-[Re(CO)$_3$(4,4′-DiMBpy)(Br)] (4)**	380	365	610	230	9922	0.67
***fac*-[Re(CO)$_3$(5,5′-DiMBpy)(Br)] (5)**	375	335	600	225	10,000	1.5
***fac*-[Re(CO)$_3$(4,4′-DiMoxBpy)(Br)] (6)**	365	365	620	255	11,268	0.35
***fac*-[Re(CO)$_3$(4,4′-DiMBpy)(PPh$_3$)]$^+$ (7)**	347	335	600	253	12,152	0.43
***fac*-[Re(CO)$_3$(4,4′-DiMBpy)(PTA)]$^+$ (8)**	361	–	–	–	–	–
***fac*-[Re(CO)$_3$(4,4′-DiMBpy)(CyPh$_2$P)]$^+$ (9)**	354	335	600	246	11,582	0.46
***fac*-[Re(CO)$_3$(4,4′-DiMBpy)(Cy$_2$PhP)]$^+$ (10)**	355	335	600	245	11,502	0.49
***fac*-[Re(CO)$_3$(5,5′-DiMBpy)(PPh$_3$)]$^+$ (11)**	350	330	600	250	11,905	1.1
***fac*-[Re(CO)$_3$(5,5′-DiMBpy)(PTA)]$^+$ (12)**	355	–	–	–	–	–
***fac*-[Re(CO)$_3$(5,5′-DiMBpy)(CyPh$_2$P)]$^+$ (13)**	352	335	600	248	11,742	0.92
***fac*-[Re(CO)$_3$(5,5′-DiMBpy)(Cy$_2$PhP)]$^+$ (14)**	356	335	605	249	11,561	0.87
***fac*-[Re(CO)$_3$(4,4′-DiMoxBpy)(PPh$_3$)]$^+$ (15)**	354	335	545	191	9900	1.0
***fac*-[Re(CO)$_3$(4,4′-DiMoxBpy)(PTA)]$^+$ (16)**	352	–	–	–	–	–
***fac*-[Re(CO)$_3$(4,4′-DiMoxBpy)(CyPh$_2$P)]$^+$ (17)**	349	335	545	196	10,305	1.1
***fac*-[Re(CO)$_3$(4,4′-DiMoxBpy)(Cy$_2$PhP)]$^+$ (18)**	357	350	580	223	10,770	0.27

*Stokes shifts [cm^{-1}] calculated from $\Delta\tilde{\nu} = \tilde{\nu}_{abs} - \tilde{\nu}_{fluo}$ of spectral maxima or weighted maxima.

Table 3
A summary of the results obtained from the screening of compound(s), *fac*-[Re(CO)$_3$(4,4′-DiMoxBpy)(Br)] (**6**) and *fac*-[Re(CO)$_3$(5,5′-DiMBpy)(CyPh$_2$P]$^+$ (**13**) against cancerous (MCF-7 and MDA-MB-231) and healthy (MRC-5) cells (with the reported cisplatin results).

Compound	Cell Line	IC_{50}	SI
***fac*-[Re(CO)$_3$(4,4′-dmoxbpy)Br] (6)**	MDA-MB-231	10.92 ± 2.3	1.49
	MRC-5	16.25 ± 1.9	–
***fac*-[Re(CO)$_3$(5,5′-dmbpy)(CyhexPh$_2$P)]$^+$ (13)**	MCF-7	5.74 ± 2.5	2.62
	MRC-5	15.04 ± 2.6	–
cisplatin	MCF-7	12 ± 2.8	1.52
	MDA-MB-231	13 ± 1.8	1.65
	MRC-5	7.9 ± 1.2	

displayed an IC_{50} value of 10.92 μM against MDA-MB-231 cancer cells and 16.25 μM against MRC-5 cells. A selectivity index (SI = 1.55) of < 2 is noted for **6** on MDA-MB-231, which unfortunately shows that the complex is not only selective towards cancer cells, but can also kill normal human cells. Furthermore, **6** seems to be less lethal towards normal cells (IC_{50} = 16.25 μM) as compared to the reported cisplatin results (IC_{50} = 7.9 ± 1.2), as seen in Table 3.

When **13** was tested against MCF-7 cells, an IC_{50} value of 5.74 μM was determined. A selectivity index (SI = 2.62) of > 2 is obtained for **13**, which shows that the complex is selective towards cancer cells and does not kill normal cells. It further indicates that **13** is more active than cisplatin, IC_{50} = 12 ± 2.8 μM, against MCF-7 breast cancer cells. When the results from this study were compared to that of the drug of choice, cisplatin, it showed that cisplatin has a remarkable selectivity in killing cancer cells, with IC_{50} values of 12 ± 2.8, 13 ± 1.8 and 7.9 ± 1.2 against MCF-7, MDA-MB-231 and MRC-5, respectively. However, it shows that cisplatin is also toxic towards healthy cells.

4. Conclusions

Eighteen complexes were successfully synthesized using the "2 + 1″ mixed ligand approach in considerably high yield and purity. Furthermore, these complexes were characterized using the spectroscopic methods IR, NMR (^{1}H, ^{13}C, ^{31}P) and UV/Vis, and three solid state crystal structures were determined using SCXRD. This proves that the synthesis methods employed in the study are accurate and reproducible. The IR carbonyl stretching frequencies assisted in observing the electron-withdrawing effects of the axially coordinated monodentate ligands. The crystal structures of *fac*-[Re(CO)$_3$(5,5′-DiMBpy)(NO$_3$)], *fac*-[Re(CO)$_3$(4,4′-DiMoxBpy)(NO$_3$)][(CH$_3$)$_2$CO] and *fac*-[Re(CO)$_3$(4,4′-DiMBpy)(Br)] allowed for a discussion on the bond distances and angles, and the π…π interactions observed in *fac*-[Re(CO)$_3$(5,5′-DiMBpy)(NO$_3$)]. Moreover, all the complexes reveal suitable luminescence intensities and, more significantly, their emission and Stokes shift indicate possible application in cancer therapy and diagnosis. The complexes of particular interest, with promising toxicity results respectively towards MCF-7 and MDA-MB-231 breast cancer cell lines, are *fac*-[Re(CO)$_3$(4,4′-DiMoxBpy)(Br)] and *fac*-[Re(CO)$_3$(5,5′-DiMBpy)(CyPh$_2$P)][NO$_3$], with comparable results to cisplatin.

CRediT authorship contribution statement

Lehlohonolo Moherane: Data curation, Writing – original draft. **Orbett T. Alexander:** Data curation, Methodology. **Marietjie Schutte-Smith:** Writing – review & editing. **Robin E. Kroon:** Data curation, Methodology. **Penny P. Mokolokolo:** Data curation, Methodology. **Supratim Biswas:** Data curation, Methodology. **Sharon Prince:** Data curation, Methodology. **Hendrik G. Visser:** Supervision, Writing – review & editing. **Amanda-Lee E. Manicum:** Supervision, Conceptualization, Methodology, Writing – original draft, Writing – review & editing.

Declaration of Competing Interest

The authors declare that they have no known competing financial interests or personal relationships that could have appeared to influence the work reported in this paper.

Data availability

Data will be made available on request.

Acknowledgment

We would like to thank the National Research Foundation (Grant No. 129468), Tshwane University of Technology, University of the Free State, South Africa, for institutional and financial support.

Appendix A. Supplementary data

Supplementary data to this article can be found online at https://doi.org/10.1016/j.poly.2022.116178.

References

[1] B.W. Henderson, Photodynamic therapy: basic principles and clinical applications, CRC Press, 2020.
[2] T.J. Dougherty, C.J. Gomer, B.W. Henderson, G. Jori, D. Kessel, M. Korbelik, J. Moan, Q. Peng, Photodynamic therapy. *JNCI*, J. Natl. Cancer Inst. 90 (1998) 889–905.
[3] R. Bonnett, Chemical aspects of photodynamic therapy, CRC Press, 2000.
[4] O. Raab, On the effect of fluorescent substances on infusoria, Z. Biol. 39 (1900) 524–526.
[5] J.M. Brown, Tumor Hypoxia in Cancer Therapy, in: Methods in Enzymology, Academic Press, 2007, pp. 295–321.
[6] A. Juzeniene, J. Moan, The history of PDT in Norway: Part one: Identification of basic mechanisms of general PDT, Photodiagnosis Photodyn. Ther. 4 (2007) 3–11.
[7] D. Álvarez, M.I. Menéndez, R. López, Computational Design of Rhenium(I) Carbonyl Complexes for Anticancer Photodynamic Therapy, Inorg. Chem. 61 (2022) 439–455.
[8] A.J. Amoroso, M.P. Coogan, J.E. Dunne, V. Fernández-Moreira, J.B. Hess, A. J. Hayes, D. Lloyd, C. Millet, S.J.A. Pope, C. Williams, Rhenium fac tricarbonyl bisimine complexes: biologically useful fluorochromes for cell imaging applications, Chem. Commun. (2007) 3066–3068.
[9] A. Kastl, S. Dieckmann, K. Wähler, T. Völker, L. Kastl, A.L. Merkel, A. Vultur, B. Shannan, K. Harms, M. Ocker, Rhenium complexes with visible-light-induced anticancer activity, ChemMedChem 8 (2013) 924–927.
[10] J. Shum, P.-K.-K. Leung, K.-K.-W. Lo, Luminescent Ruthenium(II) Polypyridine Complexes for a Wide Variety of Biomolecular and Cellular Applications, Inorg. Chem. 58 (2019) 2231–2247.
[11] K.-K.-W. Lo, Luminescent Rhenium(I) and Iridium(III) Polypyridine Complexes as Biological Probes, Imaging Reagents, and Photocytotoxic Agents, Acc. Chem. Res. 48 (2015) 2985–2995.
[12] S. Faulkner, S.J.A. Pope, B.P. Burton-Pye, Lanthanide Complexes for Luminescence Imaging Applications, Appl. Spectrosc. Rev. 40 (2005) 1–31.
[13] V. Marin, E. Holder, R. Hoogenboom, E. Tekin, U.S. Schubert, Light-emitting iridium(iii) and ruthenium(ii) polypyridyl complexes containing quadruple hydrogen-bonding moieties, Dalton Trans. (2006) 1636–1644.
[14] A. Kastl, S. Dieckmann, K. Wähler, T. Völker, L. Kastl, A.L. Merkel, A. Vultur, B. Shannan, K. Harms, M. Ocker, W.J. Parak, M. Herlyn, E. Meggers, Rhenium Complexes with Visible-Light-Induced Anticancer Activity, ChemMedChem 8 (2013) 924–927.
[15] K. Wähler, A. Ludewig, P. Szabo, K. Harms, E. Meggers, Rhenium Complexes with Red-Light-Induced Anticancer Activity, Eu. J. Inorg. Chem. (2014) 807–811.
[16] V. Fernández-Moreira, F.L. Thorp-Greenwood, M.P. Coogan, Application of d6 transition metal complexes in fluorescence cell imaging, Chem. Commun. 46 (2010) 186–202.
[17] Q. Zhao, C. Huang, F. Li, Phosphorescent heavy-metal complexes for bioimaging, Chem. Soc. Rev. 40 (2011) 2508–2524.
[18] C.C. Konkankit, S.C. Marker, K.M. Knopf, J.J. Wilson, Anticancer activity of complexes of the third row transition metals, rhenium, osmium, and iridium, Dalton Trans. 47 (2018) 9934–9974.
[19] M. Mkhatshwa, J.M. Moremi, K. Makgopa, A.-L.-E. Manicum, Nanoparticles Functionalised with Re(I) Tricarbonyl Complexes for Cancer Theranostics, Int. J. Mol. Sci. 22 (2021) 6546.
[20] D.D. Perrin, W.L. Armarego, D.R. Perrin, Purification of laboratory chemicals, 1966.
[21] R. Alberto, A. Egli, U. Abram, K. Hegetschweiler, V. Gramlich, P.A. Schubiger, Synthesis and reactivity of $[NEt_4]_2[ReBr\ 3(CO_)3]$. Formation and structural characterization of the clusters $[NE_t4][R_e3(_\mu3\text{-}OH)(\mu\text{-}OH_)3(CO_)9]$ and $[NE_t4][R_e2(\mu\text{-}OH_)3(CO_)6]$ by alkaline titration, J. Chem. Soc. Dalton Trans. (1994) 2815–2820.
[22] A.-L.-E. Manicum, M. Schutte-Smith, H.G. Visser, The synthesis and structural comparison of fac-$[Re(CO)_3]+$ containing complexes with altered β-diketone and phosphine ligands, Polyhedron 145 (2018) 80–87.
[23] A.-L. Manicum, O. Alexander, M. Schutte-Smith, H.G. Visser, Synthesis, characterization and substitution reactions of fac-[Re(O, O′-bid)$(CO_)3$(P)] complexes, using the "2+1" mixed ligand model, J. Mol. Struct. 1209 (2020), 127953.
[24] S.-P. Bruker, Version 7.12 (including XPREP), Bruker AXS Inc., Madison, Wisconsin, USA, 2004.
[25] A. Altomare, M.C. Burla, M. Camalli, G.L. Cascarano, C. Giacovazzo, A. Guagliardi, A.G.G. Moliterni, G. Polidori, R. Spagna, SIR97: A new tool for crystal structure determination and refinement, J. Appl. Crystallogr. 32 (1999) 115–119.
[26] L.J. Farrugia, WinGX suite for small-molecule single-crystal crystallography, J. Appl. Crystallogr. 32 (1999) 837–838.
[27] G. Sheldrick, Program for the refinement of crystal structures, Shelxl97 (1997).
[28] K. Brandenburg, M. Brendt, DIAMOND, Release 2.1 d 302 (2000) 303.
[29] M. Wrighton, D.L. Morse, Nature of the lowest excited state in tricarbonylchloro-1,10-phenanthrolinerhenium(I) and related complexes, J. Am. Chem. Soc. 96 (1974) 998–1003.
[30] B.L. Souza, L.A. Faustino, F.S. Prado, R.N. Sampaio, P.I.S. Maia, A.E.H. Machado, A.O.T. Patrocinio, Spectroscopic characterization of a new Re(i) tricarbonyl complex with a thiosemicarbazone derivative: towards sensing and electrocatalytic applications, Dalton Trans. 49 (2020) 16368–16379.
[31] L.S. Matos, R.C. Amaral, N.Y. Murakami Iha, Visible Photosensitization of trans-Styrylpyridine Coordinated to fac-$[Re(CO)_3(dcbH_2)](+)$: New Insights, Inorg. Chem. 57 (2018) 9316–9326.
[32] C. Triantis, T. Tsotakos, C. Tsoukalas, M. Sagnou, C. Raptopoulou, A. Terzis, V. Psycharis, M. Pelecanou, I. Pirmettis, M. Papadopoulos, Synthesis and Characterization of fac-$[M(CO)_3(P)(OO)]$ and cis-trans-$[M(CO)_2(P)_2(OO)]$ Complexes (M = Re, (99m)Tc) with Acetylacetone and Curcumin as OO Donor Bidentate Ligands, Inorg. Chem. 52 (2013) 12995–13003.
[33] V.L. Gantsho, M. Dotou, M. Jakubaszek, B. Goud, G. Gasser, H.G. Visser, M. Schutte-Smith, Synthesis, characterization, kinetic investigation and biological evaluation of Re(i) di- and tricarbonyl complexes with tertiary phosphine ligands, Dalton Trans. 49 (2020) 35–46.
[34] M.R. Gonçalves, K.P.M. Frin, Synthesis, characterization, photophysical and electrochemical properties of rhenium(I) tricarbonyl diimine complexes with triphenylphosphine ligand, Polyhedron 132 (2017) 20–27.
[35] G.E. Maciel, R.V. James, Solvent Effects on the Phosphorus-31 Chemical Shift in Triphenylphosphine Oxide, Inorg. Chem. 3 (1964) 1650–1651.
[36] A.-L.-E. Manicum, M. Schutte-Smith, O.T. Alexander, L. Twigge, A. Roodt, H. G. Visser, First kinetic data of the CO substitution in fac-[Re(L, L′-Bid)$(CO_)3$(X)] complexes (L, L′-Bid = acacetylacetonate or tropolonate) by tertiary phosphines PTA and P_Ph3: Synthesis and crystal structures of water-soluble rhenium(I) tri- and dicarbonyl complexes with 1,3,5-triaza-7-phosphaadamantane (PTA), Inorg. Chem. Commun. 101 (2019) 93–98.
[37] M.J. Moremi, O.T. Alexander, B. Vatsha, K. Makgopa, A.-L.-E. Manicum, The crystal structure of fac-tricarbonyl(4,4-dimethyl-2,2-dipyridyl-κ2N, N′)- (pyrazole-κN)rhenium(I) nitrate, $_{C1}8_{H1}6_O3_N4Re$, Z. Kristallogr. - New Cryst. Struct. 236 (2021) 33–35.
[38] M. Schutte-Smith, H.G. Visser, A. Roodt, Crystal structure of fac-hexacarbonylbisμ2-(3-carboxy-3′-carboxylato-2,2′-bipyridine)-κ3N, N′:O-dirhenium(I) tetrahydrate, $_{C3}0_{H2}2_N4_{O1}8R_e2$, Z. Kristallogr. - New Cryst. Struct. 231 (2016) 335–338.
[39] A. Brink, H.G. Visser, A. Roodt, Activation of Rhenium(I) Toward Substitution in fac-[Re(N, O′-Bid)$(CO_)3(HOC_H3)$] by Schiff-Base Bidentate Ligands (N, O′-Bid), Inorg. Chem. 52 (2013) 8950–8961.
[40] L.V. Ramoba, O.T. Alexander, H.G. Visser, A.-L.-E. Manicum, The crystal structure of fac-tricarbonyl(1,10-phenanthroline-κ2N, N′)-(pyrazole-κN)rhenium(I)nitrate, $_{C1}8_{H1}2_O3_N4Re$, Z. Kristallogr. - New Cryst. Struct. 235 (2020) 1203–1205.
[41] A.E. Miroslavov, G.V. Sidorenko, M.Y. Tyupina, V.V. Gurzhiy, $[Re(CO)_3(bipy)(ClO_4)]$: Synthesis in a Proton-Donor Solvent, Crystal, and Molecular Structure, Russ. J. Gen. Chem. 90 (2020) 2333–2337.
[42] S.R. Stoyanov, J.M. Villegas, A.J. Cruz, L.L. Lockyear, J.H. Reibenspies, D. P. Rillema, Computational and Spectroscopic Studies of Re(I) Bipyridyl Complexes Containing 2,6-Dimethylphenylisocyanide (CN_x) Ligand, J. Chem. Theory Comput. 1 (2005) 95–106.
[43] E. Hevia, J. Pérez, V. Riera, D. Miguel, S. Kassel, A. Rheingold, New Synthetic Routes to Cationic Rhenium Tricarbonyl Bipyridine Complexes with Labile Ligands, Inorg. Chem. 41 (2002) 4673–4679.
[44] L. Moherane, O.T. Alexander, H.G. Visser, A.-L.-E. Manicum, The crystal structure of [μ-hydroxido-bis[(5,5′-dimethyl-2,2′-bipyridine-κ2N, N′)-tricarbonylrhenium (I)] bromide hemihydrate, $_{C3}0_{H2}6_N4_O9R_e2Br$, Z. Kristallogr. - New Cryst. Struct. 236 (2021) 1027–1029.
[45] N.A. Lewis, P.A. Marzilli, F.R. Fronczek, L.G. Marzilli, Models for B12-conjugated radiopharmaceuticals. Cobaloxime binding to new fac-$[Re(CO)_3(Me_2bipyridine)(amidine)]B_F4$ complexes having an exposed pyridyl nitrogen, Inorg. Chem. 53 (2014) 11096–11107.
[46] R. Kia, F. Safari, Synthesis, spectral and structural characterization and computational studies of rhenium(I)-tricarbonyl nitrito complexes of 2,2′-bipyridine and 2,9-dimethylphenanthroline ligands: π-Accepting character of the diimine ligands, Inorg. Chim. Acta 453 (2016).
[47] M. Schutte, G. Kemp, H.G. Visser, A. Roodt, Tuning the reactivity in classic low-spin d6 rhenium(I) tricarbonyl radiopharmaceutical synthon by selective bidentate ligand variation (L, L'-Bid; L, L'= N, N', N, O, and O, O' donor atom sets) in fac-[Re(CO)3(L, L'-Bid)(MeOH)]n complexes, Inorg. Chem. 50 (2011) 12486–12498.
[48] E. Hevia, J. Pérez, V. Riera, D. Miguel, New Octahedral Rhenium(I) Tricarbonyl Amido Complexes, Organometallics 21 (2002) 1966–1974.
[49] H.-Y. Li, J. Wu, X.-H. Zhou, L.-C. Kang, D.-P. Li, Y. Sui, Y.-H. Zhou, Y.-X. Zheng, J.-L. Zuo, X.-Z. You, Synthesis, structural characterization and photoluminescence properties of rhenium(I) complexes based on bipyridine derivatives with carbazole moieties, Dalton Trans. (2009) 10563–10569.
[50] Z. Si, J. Li, B. Li, F. Zhao, S. Liu, W. Li, Synthesis, structural characterization, and electrophosphorescent properties of rhenium(I) complexes containing carrier-transporting groups, Inorg. Chem. 46 (15) (2007) 6155–6163.
[51] K. Koike, J. Tanabe, S. Toyama, H. Tsubaki, K. Sakamoto, J.R. Westwell, F. P. Johnson, H. Hori, H. Saitoh, O. Ishitani, New synthetic routes to biscarbonylbipyridinerhenium(I) complexes cis, trans-$[Re(_X2bpy)(CO_)2(P_R3)(Y^)n+$ ($_X2bpy$ = 4,4'-$_X2$-2,2'-bipyridine) via photochemical ligand substitution reactions, and their photophysical and electrochemical properties, Inorg. Chem. 39 (2000) 2777–2783.
[52] M.V. Werrett, D. Chartrand, J.D. Gale, G.S. Hanan, J.G. MacLellan, M. Massi, S. Muzzioli, P. Raiteri, B.W. Skelton, M. Silberstein, S. Stagni, Synthesis, structural, and photophysical investigation of diimine tricarbonyl Re(I) tetrazolato complexes, Inorg. Chem. 50 (2011) 1229–1241.

[53] M.L. Waters, Aromatic interactions in model systems, Curr. Opin. Chem. Biol. 6 (2002) 736–741.
[54] Y. Zhao, J. Li, H. Gu, D. Wei, Y.C. Xu, W. Fu, Z. Yu, Conformational Preferences of π-π Stacking Between Ligand and Protein, Analysis Derived from Crystal Structure Data Geometric Preference of π-π Interaction, Interdiscip. Sci. Comput. Life Sci. 7 (2015) 211–220.
[55] M. Wolff, L. Munoz, A. François, C. Carrayon, A. Seridi, N. Saffon, C. Picard, B. Machura, E. Benoist, Tricarbonylrhenium complexes from 2-pyridyl-1,2,3-triazole ligands bearing a 4-substituted phenyl arm: a combined experimental and theoretical study, Dalton Trans. 42 (2013) 7019–7031.
[56] S. Ranjan, S.-Y. Lin, K.-C. Hwang, Y. Chi, W.-L. Ching, C.-S. Liu, Y.-T. Tao, C.-H. Chien, S.-M. Peng, G.-H. Lee, Realizing Green Phosphorescent Light-Emitting Materials from Rhenium(I) Pyrazolato Diimine Complexes, Inorg. Chem. 42 (2003) 1248–1255.
[57] A.J. Blake, N.R. Champness, T.L. Easun, D.R. Allan, H. Nowell, M.W. George, J. Jia, X.-Z. Sun, Photoreactivity examined through incorporation in metal−organic frameworks, Nat. Chem. 2 (2010) 688–694.
[58] K.P.M. Frin, R.M. de Almeida, Mono- and di-nuclear Re(i) complexes and the role of protonable nitrogen atoms in quenching emission by hydroquinone, Photochem. Photobiol. Sci. 16 (2017) 1230–1237.
[59] K.-K.-W. Lo, M.-W. Louie, K.-S. Sze, J.-S.-Y. Lau, Rhenium(I) Polypyridine Biotin Isothiocyanate Complexes as the First Luminescent Biotinylation Reagents: Synthesis, Photophysical Properties, Biological Labeling, Cytotoxicity, and Imaging Studies, Inorg. Chem. 47 (2008) 602–611.
[60] S.C. Marker, S.N. MacMillan, W.R. Zipfel, Z. Li, P.C. Ford, J.J. Wilson, Photoactivated in Vitro Anticancer Activity of Rhenium(I) Tricarbonyl Complexes Bearing Water-Soluble Phosphines, Inorg. Chem. 57 (2018) 1311–1331.
[61] M.S. Capper, A. Enriquez Garcia, N. Macia, B. Lai, J.B. Lin, M. Nomura, A. Alihosseinzadeh, S. Ponnurangam, B. Heyne, C.S. Shemanko, F. Jalilehvand, Cytotoxicity, cellular localization and photophysical properties of Re(I) tricarbonyl complexes bound to cysteine and its derivatives, J. Biol. Inorg. Chem. 25 (2020) 759–776.
[62] T. Morimoto, O. Ishitani, Modulation of the Photophysical, Photochemical, and Electrochemical Properties of Re(I) Diimine Complexes by Interligand Interactions, Acc. Chem. Res. 50 (2017) 2673–2683.
[63] J. Bhuvaneswari, P.M. Mareeswaran, K. Anandababu, S. Rajagopal, The switching of a Rhenium(i) complex from turn-off to turn-on sensor system through protein binding, RSC Adv. 4 (2014) 34659–34668.
[64] H.S. Liew, C.-W. Mai, M. Zulkefeli, T. Madheswaran, L.V. Kiew, N. Delsuc, M. L. Low, Recent Emergence of Rhenium(I) Tricarbonyl Complexes as Photosensitisers for Cancer Therapy, Molecules 25 (2020) 4176.
[65] L. Sacksteder, A.P. Zipp, E.A. Brown, J. Streich, J.N. Demas, B.A. DeGraff, Luminescence studies of pyridine.alpha.-diimine rhenium(I) tricarbonyl complexes, Inorg. Chem. 29 (1990) 4335–4340.
[66] L.-C.-C. Lee, K.-K. Leung, K.-K.-W. Lo, Recent development of luminescent rhenium (i) tricarbonyl polypyridine complexes as cellular imaging reagents, anticancer drugs, and antibacterial agents, Dalton Trans. 46 (2017) 16357–16380.
[67] M.P. Coogan, V. Fernández-Moreira, Progress with, and prospects for, metal complexes in cell imaging, Chem. Commun. 50 (2014) 384–399.
[68] L. He, Z.-Y. Pan, W.-W. Qin, Y. Li, C.-P. Tan, Z.-W. Mao, Impairment of the autophagy-related lysosomal degradation pathway by an anticancer rhenium(i) complex, Dalton Trans. 48 (2019) 4398–4404.
[69] A.J. Winstead, K. Alabrash, B.V. Powell, S.J. Parnell, T.V. Hinton, T. Odebode, J. Peng, J.A. Krause, P.Y. Zavalij, S.K. Mandal, Microwave-Assisted Synthesis of Organometallic Rhenium (I) Pentylcarbonato Complexes: New Synthon for Carboxylato, Sulfonato and Chlorido Complexes, J. Organomet. Chem. 936 (2021), 121718.
[70] P. Collery, A. Mohsen, A. Kermagoret, S. Corre, G. Bastian, A. Tomas, M. Wei, F. Santoni, N. Guerra, D. Desmaële, J. d'Angelo, Antitumor activity of a rhenium (I)-diselenoether complex in experimental models of human breast cancer, Invest. New Drugs 33 (2015) 848–860.
[71] A. Leonidova, G. Gasser, Underestimated potential of organometallic rhenium complexes as anticancer agents, ACS Chem. Biol. 9 (2014) 2180–2193.
[72] M.K. Mbagu, D.N. Kebulu, A.J. Winstead, S.K. Pramanik, H.n. Banerjee, M. O. Iwunze, J. Wachira, G.E. Greco, G.K. Haynes, A. Sehmer, F.H. Sarkar, D.M. Ho, R.D. Pike, S.K. Mandal, Fac-tricarbonyl(pentylcarbonato)+±-diimine)rhenium complexes: One-pot synthesis, characterization, fluorescence studies, and cytotoxic activity against human MDA-MB-231 breast, CCl-227 colon and BxPC-3 pancreatic carcinoma cell lines, Inorg. Chem. Commun. 21 (2012) 35–38.
[73] F.X. Wang, J.H. Liang, H. Zhang, Z.H. Wang, Q. Wan, C.P. Tan, L.N. Ji, Z.W. Mao, Mitochondria-Accumulating Rhenium(I) Tricarbonyl Complexes Induce Cell Death via Irreversible Oxidative Stress and Glutathione Metabolism Disturbance, ACS Appl. Mater. Interfaces 11 (2019) 13123–13133.
[74] Z.-Y. Pan, D.-H. Cai, L. He, Dinuclear phosphorescent rhenium(i) complexes as potential anticancer and photodynamic therapy agents, Dalton Trans. 49 (2020) 11583–11590.
[75] L.D. Ramos, L.H. de Macedo, N.R.S. Gobo, K.T. de Oliveira, G. Cerchiaro, K. P. Morelli Frin, Understanding the photophysical properties of rhenium(i) compounds coordinated to 4,7-diamine-1,10-phenanthroline: synthetic, luminescence and biological studies, Dalton Trans. 49 (2020) 16154–16165.
[76] R. Paprocka, M. Wiese-Szadkowska, S. Janciauskiene, T. Kosmalski, M. Kulik, A. Helmin-Basa, Latest developments in metal complexes as anticancer agents, Coord. Chem. Rev. 452 (2022), 214307.
[77] J. Delasoie, A. Pavic, N. Voutier, S. Vojnovic, A. Crochet, J. Nikodinovic-Runic, F. Zobi, Identification of novel potent and non-toxic anticancer, anti-angiogenic and antimetastatic rhenium complexes against colorectal carcinoma, Eur. J. Med. Chem. 204 (2020), 112583.